Available online at www.sciencedirect.com
ScienceDirect
Ceramics International 37 (2011) 2477–2484
CERAMICS INTERNATIONAL
www.elsevier.com/locate/ceramint

$Y_3Al_5O_{12}$ translucent nanostructured ceramics—Obtaining and optical properties

R.P. Yavetskiy [a,*], E.A. Vovk [a], A.G. Doroshenko [a], M.I. Danylenko [b], A.V. Lopin [a], I.A. Petrusha [c], V.F. Tkachenko [a], A.V. Tolmachev [a], V.Z. Turkevich [c]

[a] *Institute for Single Crystals, STC "Institute for Single Crystals", NAS of Ukraine, 60 Lenin Ave., 61001, Kharkov, Ukraine*
[b] *Frantsevich Institute for Problems of Materials Sciences, NAS of Ukraine, 3 Krzhizhanovskoho Str., 03680, Kyiv, Ukraine*
[c] *Bakul Institute for Superhard Materials, NAS of Ukraine, 2 Avtozavodskaya Str., 04074, Kyiv, Ukraine*

Received 23 February 2011; accepted 29 March 2011
Available online 8 April 2011

Abstract

$Y_3Al_5O_{12}$ nanostructured ceramics with total transmittance of 63% at $\lambda = 1064$ nm has been obtained by low-temperature high-pressure sintering. According to high-resolution transmission electron microscopy ceramics is near pore-free and consists of close-packed grains of 20–40 nm in size. The transmittance spectrum in the visible and IR wavelength range, stationary X-ray excited luminescence and thermally stimulated luminescence were studied to characterize $Y_3Al_5O_{12}$ nanostructured ceramics in comparison to single crystals of the same composition. The observed differences in the optical and luminescent properties were interpreted as a consequence of high defectivity level of nanoceramics arising from its non-equilibrium character, extremely large concentration of grain boundaries and surface states.

Keywords: A. Sintering; E. Functional application; Optical materials; $Y_3Al_5O_{12}$

1. Introduction

The development of new functional materials on the basis of transparent polycrystalline materials is one of the most important achievements of the modern luminescent material science [1]. The best progress was obtained for traditional laser materials such as $Y_3Al_5O_{12}$ [2–4] and rare earth sesqioxides RE_2O_3 (RE = Y, Sc, Gd, Lu) [5] activated by Ln^{3+} ions. These materials are optically isotropic thus do not demonstrate light scattering on randomly oriented grains of ceramics. Nowadays optical ceramics is considered as a promising class of materials for phosphors [6], transparent armor [7], scintillation detectors [8], etc. To achieve optical transmittance compared to those for single crystals with corresponding composition the extremely low porosity of about 10^{-2} to 10^{-3} vol.% is required. Such porosity levels traditionally could be obtained via prolonged sintering at high temperatures resulting in grain growth up to hundreds of microns. It is usually assumed that higher grain size promote higher transparency levels due to lower density of grain boundaries and triple junction. However, recent results indicate that low residual porosity is much more critical parameter to attain high transparency. For example, even for alumina non-isotropic ceramics grain size decrease leads to transmittance increase [9,10]. Moreover, decrease of grain size also improves mechanical properties of ceramics [11].

The traditional approach to the development of optical ceramics is based on the use of hot isostatic pressing or vacuum sintering of nanopowders. The sintering is performed at rather high temperatures (~0.7–0.8 T_{melt}) resulting in coarse-grained ceramics. An alternative method to produce optical ceramics implies the retaining of their nanostructure, when grains are much finer than the visible light wavelength. Nowadays transparent 2D nanomaterials are known, in particular sol–gel films. Obtaining of transparent bulk nanoceramics is a significant challenge, because during consolidation of nanocrystalline powders the grain size in the nanometer range should be maintained. Several rapid sintering routes enable fabrication of translucent nanostructured ceramics. Typical examples are translucent YSZ ceramics was obtained by current activated sintering technique [12,13] and $Y_3Fe_5O_{12}$

* Corresponding author. Tel.: +380 57 341 0415; fax: +380 57 340 9343.
E-mail address: yavetskiy@isc.kharkov.ua (R.P. Yavetskiy).

0272-8842/$36.00
doi:10.1016/j.ceramint.2011.03.041

produced by high-pressure torsion of coarse powders [14]. Low-temperature high-pressure sintering is another effective methods for fabrication of optical nanostructured materials, such as Al_2O_3 [15], $MgAl_2O_4$ [16–18], $Y_3Al_5O_{12}$ [19] and Lu_2O_3 [20].

It is known that nanostructured ceramics with grain size from 100 to 10 nm have 10–50% of atoms within grain boundaries. As a result, optical and electronic properties of nanoceramics are substantially different compared to bulk materials. For instance, nanostructured Al_2O_3 shows new luminescence band originated from surface F_S^+-centers; has faster luminescence decay and higher luminescence yield compared to corresponding single crystals [21]. $MgAl_2O_4$ nanostructured ceramics reveals blue shift of IR cutoff wavelength [16]. Differences in optical properties of the nano- and single-crystalline form of $Y_3Fe_5O_{12}$ were observed in [22]. Studies of luminescent properties of $Y_3Al_5O_{12}$ nanoceramics are limited by activated materials [23–26]. Optical properties of nominally pure $Y_3Al_5O_{12}$ nanoceramics are purely presented in modern literature. The aim of this work was to obtain $Y_3Al_5O_{12}$ optical nanostructured ceramics by low-temperature high-pressure sintering and to study its optical and luminescent properties. $Y_3Al_5O_{12}$ is not only an attractive model object due to well-known optical properties for the bulk form, but also excellent laser [1–4] and scintillation material [27–29].

2. Experimental

2.1. Obtaining of $Y_3Al_5O_{12}$ nanostructured ceramics

$Y_3Al_5O_{12}$ nanocrystalline powders were produced by reverse strike co-precipitation method from 0.5 M solutions of yttrium $Y(NO_3)_3{\cdot}6H_2O$ (high purity grade) and aluminum $Al(NO_3)_3{\cdot}6H_2O$ (high purity grade) nitrates using ammonium bicarbonate NH_4HCO_3 (chemically pure) as a precipitant and further calcination of amorphous precursor in the 800–1200 °C temperature range. In some cases sulfate ions were added to the reaction mixture as a dispersant [30]. The mean size of the $Y_3Al_5O_{12}$ powder particles was found by transmission electron microscopy and from the particle specific surface (S_{BET}), measured from low-temperature nitrogen adsorption (the BET method).

The nanopowders were consolidated under the thermobaric static conditions at a toroid-type high-pressure apparatus. Before placing into the high-pressure cell the initial $Y_3Al_5O_{12}$ nanopowders were uniaxially compacted in a steel mold at a pressure of 250 MPa into pellets of 6 mm in diameter and 2.5 mm in height. The pellet density was 47–50% from the theoretical density of $Y_3Al_5O_{12}$. The pellet was placed in a capsule of chemically inert hexagonal boron nitride, which was used to ensure the quasi-hydrostatic compression of a sample and to prevent its contact with a graphite heater. The consolidation was conducted at pressures of 6–7.7 GPa and temperatures of the range from 250 to 550 °C. The isothermal holding time in experiments was 30–60 s.

2.2. Characterization of ceramics

The density of consolidated samples was assessed using hydrostatic weighing. The X-ray diffraction analysis was performed by the powder diffraction on a DRON-2.0 diffractometer in the cobalt anode radiation, $\lambda = 0.17902$ nm. The crystallite sizes of the initial powders and in the resultant ceramics were defined by the approximation method. The ceramics microstructure was studied by high-resolution analytical transmission electron microscopy (HR TEM) on a JEM-2100F (JEOL) microscope with an INCA (Oxford Instruments) X-ray microanalyzer. Samples for the HR TEM were prepared by ion thinning. For the optical measurements of ceramics 1 mm thick plates polished on both sides were used. The total spectral transmittance of samples in the 250–1100 nm wavelength range was determined on a Perkin-Elmer "Lambda-35" spectrophotometer using integrating sphere. The stationary radioluminescence was studied on an automated SDL-2 setup (LOMO) under excitation with a REIS-I X-ray tube (Cu anticathode, $U = 30$ kV) at room temperature. The TSL glow curves were recorded using a home-made setup equipped with a FEU-79 PMT at a heating rate of 5 K/min. The samples were irradiated with X-quanta (RUP150/300-10-1 X-ray unit, Cu anode; $U = 160$ kV, $I = 9$ mA) at room temperature.

3. Results and discussion

3.1. Fabrication conditions of YAG nanostructured ceramics

3.1.1. Influence of applied pressure and temperature

The specific surface of the initial $Y_3Al_5O_{12}$ nanopowders produced by calcination of precursor at 1100 °C for 2 h was $S_{BET} \approx 35$ m^2/g and the mean particle size was $d_{mean} \approx 38.5$ nm, found by the BET method. According to the electron microscopy, the average particle diameter of powders is 40–50 nm. Thus, the average particle diameters obtained by different methods agree well, which in particular can point to a low degree of powders agglomeration. The $Y_3Al_5O_{12}$ ceramics with various phase compositions, microstructures, and optical characteristics were prepared by the consolidation of nanopowders using low-temperature high-pressure sintering. As the temperature of the thermobaric action increases from 250 to 550 °C, the density of ceramics increases

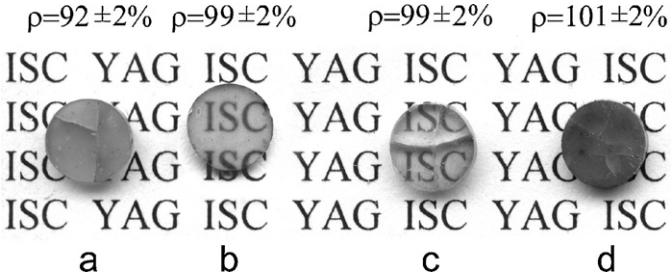

Fig. 1. $Y_3Al_5O_{12}$ nanostructured ceramics produced by low-temperature sintering for 30 s at a pressure of ~7.7 GPa and a temperature of 250 °C (a), 350 °C (b), 450 °C (c), and 550 °C (d). The pellets are 1 mm thick.

from 92 ± 2% to 101 ± 2% of the $Y_3Al_5O_{12}$ theoretical density (Fig. 1). The density higher than the theoretical value of $Y_3Al_5O_{12}$ (ρ = 4.55 g/cm^3) for the sample sintered at 550 °C is caused by pressure-induced formation of small amount of $YAlO_3$ phase (ρ = 5.35 g/cm^3), as will be shown below. Under the action of a pressure of ~7.7 GPa and temperatures of 350–450 °C there forms transparent ceramics with a density of 99 ± 2% (Fig. 1). With the traditional method of vacuum sintering to obtain the $Y_3Al_5O_{12}$ ceramics having such a density is possible only at temperatures above 1700 °C [31]. Under high pressures a considerable decrease of temperatures required for the production of the high-density ceramics from the initial nanodispersed powders is caused by the activation of the consolidation process thanks to the intense compression of the sample. It should be noted that the value of the applied pressure is comparable to that of capillary pressures in nanopowders (0.5–5 GPa). The pressure makes an essential additional contribution to the motive force of the diffusion-controlled consolidation. With the use of lower pressures the sample transparency decreased. The observed material turbidity, which is caused by the light scattering in the structure, in all likelihood stems from the formation of a considerable amount of large pores.

The influence of sintering temperature on the phase composition of obtained nanostructured ceramics is presented in Fig. 2. $Y_3Al_5O_{12}$ samples produced at a pressure of ~7.7 GPa and temperatures of 350 and 450 °C are single-phase: the X-ray diffraction patterns exhibit lines that correspond to the cubic phase of garnet (Fig. 2b and c). At the same time except for the garnet phase, whose content was 92 wt.%, the $YAlO_3$ orthorhombic phase (5–8 wt.%) was also revealed in the sample produced at 550 °C (Fig. 2d). From this fact it follows that the increase of the consolidation temperature to 550 °C under the high pressure conditions results in the decomposition of $Y_3Al_5O_{12}$. The decomposition of the $Y_3Al_5O_{12}$ garnet phase into yttrium–aluminum perovskite $YAlO_3$ and aluminum oxide Al_2O_3 according to the scheme $Y_3Al_5O_{12} \rightarrow 3YAlO_3 + Al_2O_3$ was also reported in [32]. However, in the diffraction pattern from the ceramics sintered at 550 °C no diffraction lines of aluminum oxide were observed, probably because its concentration was below the X-ray diffraction method detection limit. The presence of foreign phases with a crystalline structure and the refractive index that differ from those of the basic phase results in a considerable light scattering at the interfaces and the loss of the transparency by the ceramics produced at 550 °C (Fig. 1d).

According to the X-ray analysis, the average crystallite size (D) of $Y_3Al_5O_{12}$ initial nanopowders is ~15 nm. The high pressure causes a decrease in the crystallite size at relatively low temperatures of thermobaric action. With increasing sintering temperature the D value increases and with T = 550 °C becomes comparable to that of the initial powders (D = 14 nm). A decrease of the crystallite size of the ceramics may be caused by the high pressure-induced deformation of nanocrystals, which relax, e.g., through the formation of twins (it should be noted that the dislocation plasticity of $Y_3Al_5O_{12}$ is hindered). The formation of twin interlayers may occur by the crowdion mechanism [33]. The material deformation under high stresses and low temperatures was successfully interpreted with allowance made for this mechanism. It is possible that this mechanism takes place in cold pressing of nanopowders as well [33]. An increase of the crystallite size with increasing consolidation temperature occurs probably because of the healing of the crystal structure defects and as a result of the primary recrystallization.

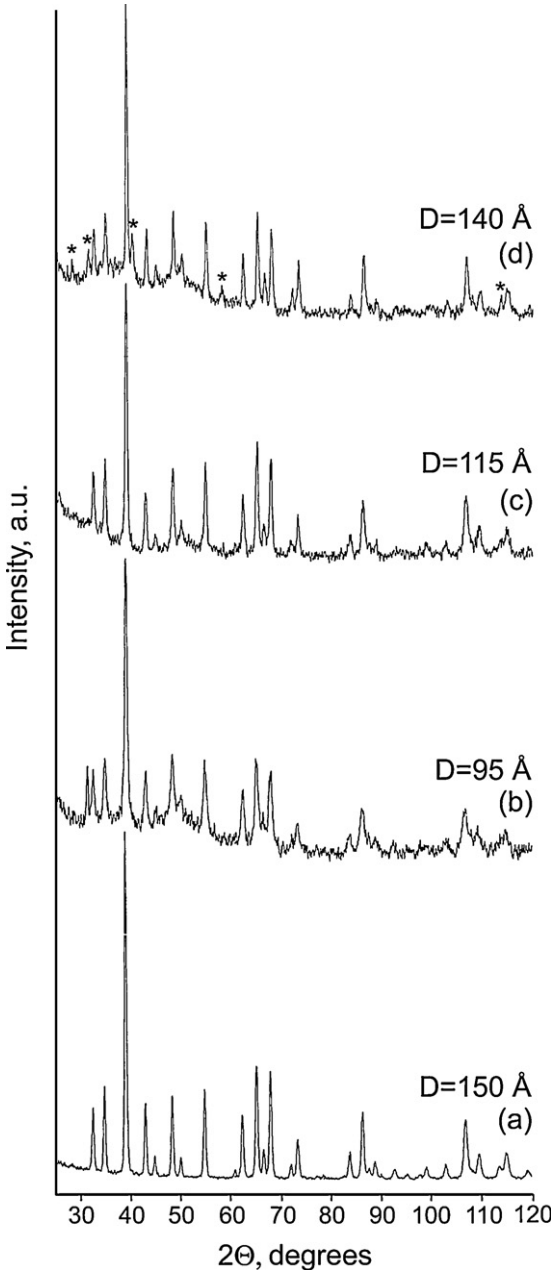

Fig. 2. X-ray diffraction patterns of $Y_3Al_5O_{12}$ initial nanopowders (a) and $Y_3Al_5O_{12}$ nanostructured ceramics sintered for 30 s at a pressure of ~7.7 GPa and a temperature of 350 °C (b), 450 °C (c), and 550 °C (d); *indicates $YAlO_3$.

3.1.2. HR TEM study

HR TEM data suggest that the resultant $Y_3Al_5O_{12}$ ceramics is nanostructured with grains of size below 100 nm (Fig. 3). Pores of submicron and micron size, which are the basic centers

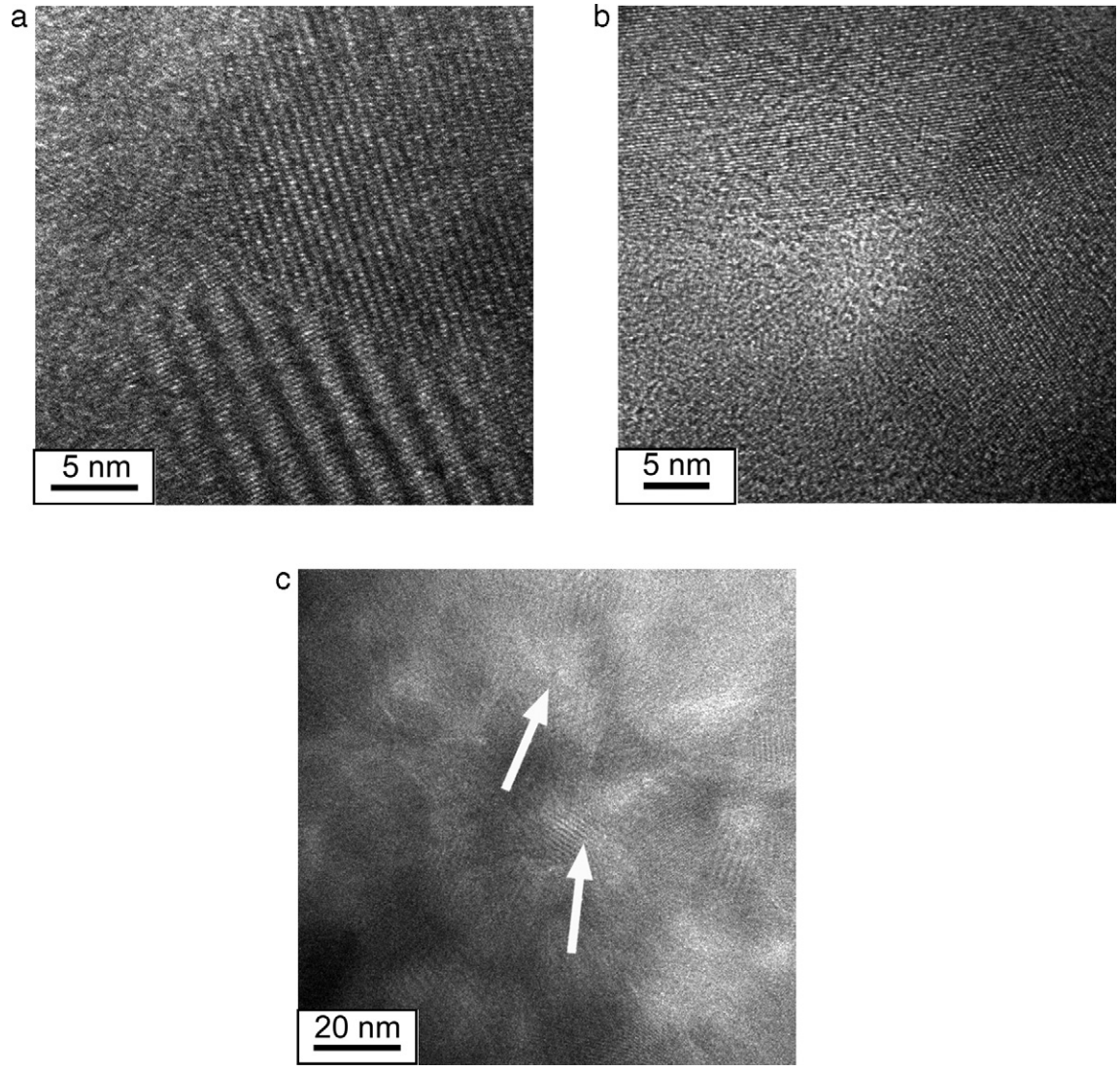

Fig. 3. Microstructure of $Y_3Al_5O_{12}$ nanoceramics sintered for 30 s at a pressure of ~7.7 GPa and 450 °C: (a) multifaceted grain boundaries with facets of arbitrary orientation; (b) a nanopore in a triple junction; (c) clusters of vacancies inside grain boundaries (the arrows indicate regions of a reduced density).

of the light scattering [13,34], are practically entirely absent in the material. In our opinion this is one of the main factors that affect the optical transmission of the $Y_3Al_5O_{12}$ nanostructured ceramics. The grain size of ceramics does not virtually change with variations of temperature, pressure, and holding time, and the grain growth factor in the consolidation does not exceed a unit for all thermobaric conditions. The mean grain size of the $Y_3Al_5O_{12}$ nanostructured ceramics in various sample regions is between 20 and 40 nm (see Fig. 3a). These values are comparable and even below than the particle size of the initial powder. The microanalysis of the element distribution indicates that the $Y_3Al_5O_{12}$ stoichiometry is retained both inside the grains and at the boundaries. Thus, in the consolidation of nanopowders at high pressures no noticeable grain growth takes place, which is clearly explained by low temperatures and short times of the process.

A perfection of grain boundaries strongly influences optical properties of ceramics with micron-sized grains. Grain boundaries in highly transparent ceramics (comparable to single crystals in optical properties) are twinned [35,36], which ensures the transparence of boundaries for quanta of light and injected acoustic phonons. Thickness of boundaries in most perfect samples is 0.2–0.5 nm, which is less than half the $Y_3Al_5O_{12}$ lattice parameter [37,38]. A comprehensive analysis of the $Y_3Al_5O_{12}$ ceramics microstructure by HRTEM has allowed us to detect that grain boundaries in nanostructures ceramics are high-angle multifaceted grain boundaries with arbitrary orientated facets (Fig. 3a). These are non-equilibrium boundaries that are characterized by a rather low density of coincident nodes (as compared to coherent boundaries) and variable angles. The width of boundaries ranges from 1 to 2 nm, which is comparable with the $Y_3Al_5O_{12}$ lattice parameter (a = 1.20089 nm). A similar structure of grain boundaries was revealed in other types of nanostructured materials as well, e.g., in TiO_2 [39].

In triple junctions between grains nanosized pores are observed, whose mean size is 3–7 nm (Fig. 3b). The capillary pressure in such pores is as high as several GPa and the external

pressure applied turns out to be insufficient to close them. One of the reasons for the formation of the residual nanoporosity may be the inhibition of the consolidation by large pores in agglomerated powders. In some areas of nanoceramics clusters of vacancies inside the grain boundaries were revealed. Such areas possess less density than grains, as evidenced by a brighter contrast in images (Fig. 3c). The clusters are one of typical defects in nanocrystalline materials which could be revealed by positron annihilation method [40]. In [24] it was assumed that under action of high pressure grains between $Y_3Al_5O_{12}$ nanocrystallites become partially amorphous, thus forming core-shell-like grain structure ''crystalline core/amorphous shell'', where amorphous layer is up to 10 nm thick. However, according to modern considerations, the grain boundaries in nanostructured materials are practically the same as in conventional polycrystals [11]. The amorphization observed in [24] most likely indicates to an incomplete densification (large pores between grains).

3.2. Optical properties of YAG nanostructured ceramics

3.2.1. Optical transmittance

Fig. 4 shows the total transmittance spectrum of transparent samples of roughly polished $Y_3Al_5O_{12}$ nanostructured ceramics. The transmittance of 63% at $\lambda = 1064$ nm represents 75% of theoretical value (84% in the visible wavelength range). The formation of the translucence in the nanostructured ceramics is obviously caused by a near full density of ceramics and decrease of the pore size below the limit, at which they scatter light. According to the model proposed in [41] for the description of optical properties of nanoporous objects, the light scattering by pores of size l can be neglected, if for given wavelength λ the size parameter $\chi = \pi l/\lambda$ is much less than 1. This means that for each wavelength there is a certain critical size of pores, below which they do not scatter the light. The combination of this condition with the data on the spectral transmission band of $Y_3Al_5O_{12}$ (>80% for $\lambda = 250$–6500 nm) allows us to formulate the criterion for transparency of nanostructured ceramics $Y_3Al_5O_{12}$. It should not contain pores of size above 10 nm. This will make it possible to avoid the light scattering by residual pores over the whole range of the ceramics transparency. Residual porosity is another factor, governing the transparency due to large difference in refractive index between the ceramics and gas-filled pores. The maximal scattering occurs when the pore size is equal to the wavelength of incident light [9]. In our case pores are as small as 10 nm, Fig. 3. However, theoretical calculations predict significant degradation of optical properties even for the pore size of 10 nm when their concentration is higher than 1% [13]. Measured density of $Y_3Al_5O_{12}$ transparent nanostructured ceramics of $99 \pm 2\%$ is close to theoretical value, indicating that another mechanisms of light scattering exist in our samples, namely light absorption by microdefects or additional scattering of light by rough surfaces of ceramics. Summarizing, transparency of nanostructured ceramics could be achieved maintaining the near full density (>99.9%) and pore size below some critical limit of about 10 nm (see, for example, [9,13]).

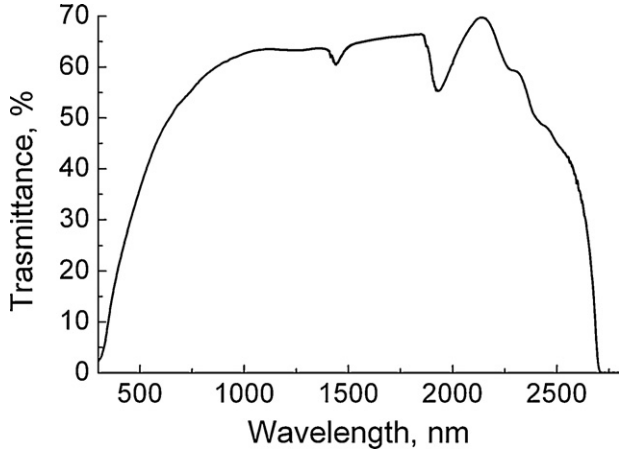

Fig. 4. Total transmittance of 1 mm thick $Y_3Al_5O_{12}$ nanostructured ceramics sintered for 60 s at a pressure of ~7.7 GPa and temperature of 350 °C.

A red shift of fundamental absorption of $Y_3Al_5O_{12}$ nanostructured ceramics is most likely caused by the ceramics coloration, whose nature is being clarified. As a possible reason for the yellow coloration of garnet crystals the uncontrolled impurities of two-valence cations (mainly calcium and magnesium), which form complex centers of coloration with matrix oxygen ions, may be considered. We should take note to significant blue shift of IR cutoff wavelength, similar to that observed for $MgAl_2O_4$ nanostructured ceramics [16]. The transmittance cutoff of $Y_3Al_5O_{12}$ in the IR is at 2.7 mkm in nanoceramics (Fig. 4) and at 6.0 mkm in single crystals. The observed red shift of fundamental absorption and blue shift of IR cutoff could point out on an increased defectivity of nanoceramics. The nanomaterials are characterized by deep level of defectivity caused by their non-equilibrium character, extremely high grain boundaries length and high fraction of surface states [42]. Uncontrolled defects, and, probably, forbidden transitions appearing from local symmetry reduction could contribute to observed reduction of transparency range. It is known that the IR cutoff in transmission of inorganic materials is determined by multi-phonon spectrum of lattice vibrations. Nanocrystalline materials possess higher density of vibration states compared to singe-crystalline ones [43]. Taking into account the large number of atoms near grain boundaries, bulk nanostructured ceramics can be considered as a community of close-packed nanograins. Thus, the shift of IR cutoff is most probably caused by modification of phonon spectrum of lattice vibrations. $Y_3Al_5O_{12}$ nanostructured ceramics contains two additional absorption bands in IR wavelength range at 1400 and 1900 nm of undefined nature. Similar absorption bands attributed to Al^{3+} ions were observed as well in $MgAl_2O_4$ nanoceramics [16].

3.2.2. Luminescence under X-ray excitation

The luminescence of $Y_3Al_5O_{12}$ single crystals under high-energy excitation originate from different luminescent centers, namely (1) self-trapped excitons (STE); (2) excitons localized near Y_{Al}^{3+} ''antisite defects'' ($LE(Y_{Al}^{3+})$); (3) ''antisite defects'' (Y_{Al}^{3+}) itself, and (4) F-like centers (one or two electron trapped by oxygen vacancy) [44–46]. Fig. 5 presents

typical normalized spectra of stationary X-ray luminescence of $Y_3Al_5O_{12}$ single crystals and nanostructured ceramics. Single crystals were grown by modified Bridgman method in Institute for Single Crystals. X-ray luminescence of single crystal is presented by three bands with maximums at λ = 310, 340 and 390 nm, corresponding to luminescence of LE(Y_{Al}^{3+}), Y_{Al}^{3+} and F-like centers (Fig. 5a). Radioluminescence of $Y_3Al_5O_{12}$ nanostructured ceramics is presented by broad band in the 300–450 nm wavelength range in which with two elementary bands at 340 and 385 nm can be distinguished (Fig. 5b). These bands correspond to luminescence of ''antisite defects'' and F-like centers, correspondingly. The position of bands is almost the same as in single crystals. We have not observed luminescence from STE in nanostructured ceramics as well in single crystals. In the undoped samples emission of STE is suppressed, probably, due to the presence of high concentration of ''antisite defects'' [44]. The UV luminescence band connected to radiative relaxation of excitons localized on Y_{Al}^{3+}-defects is totally quenched in nanoceramics probably, due to self-absorption by color centers or by matrix (Fig. 4). Thereby, we have observed formation of identical luminescence centers in bulk and nanostructured $Y_3Al_5O_{12}$. The short range ordering of atoms and formed structure in nanoceramics provides excitation mechanisms analogous to those existing in single crystals.

The relative intensity of luminescence band caused by Y_{Al}^{3+} substitution defects in nanostructured ceramics equals to that for single crystals. However, luminescence of F-like centers in nanostructured ceramics increases by the factor of 1.6 (Fig. 5b) indicating higher concentration of anionic defects. At the same time, integral luminescence yield of nanoceramics is 5 times smaller compared to single crystals of the same dimensions, probably, due to the presence of effective recombination channels through surface states. The detailed results on luminescent studies of $Y_3Al_5O_{12}$ nanostructured ceramics will be published elsewhere.

3.2.3. TSL study

Taking into account extremely high extension of grain boundaries and increased concentration of point defects in nanostructured ceramics, one can assume that defect structure of ceramics could be revealed in luminescent recombination processes, such as thermally stimulated luminescence (TSL). Fig. 6 shows TSL glow curves of $Y_3Al_5O_{12}$ single crystals and nanoceramics, obtained at heating rate of 5 K/min after

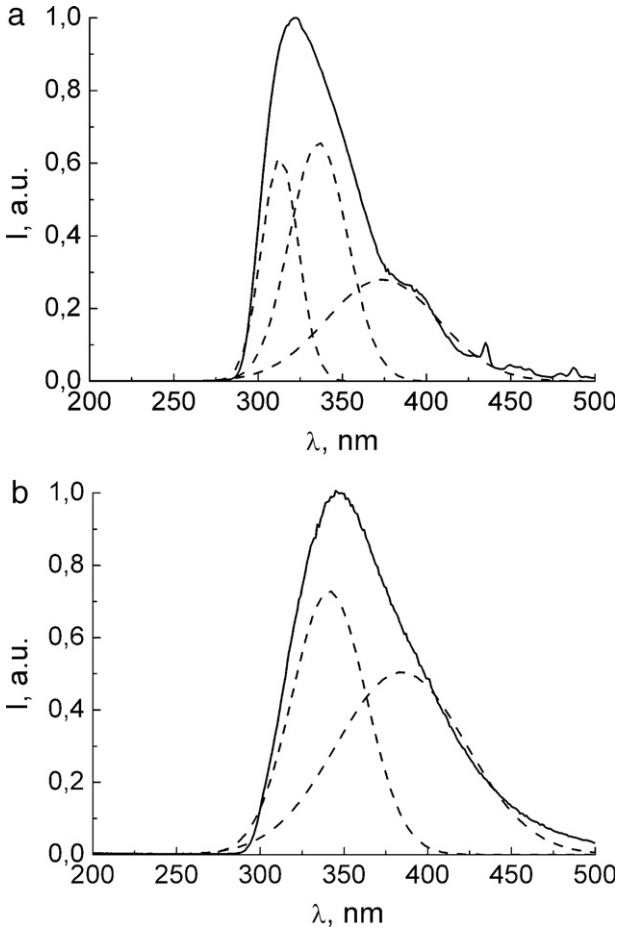

Fig. 5. Normalized room-temperature spectra of stationary X-ray luminescence (E = 30 keV) of $Y_3Al_5O_{12}$ single crystal (a) and $Y_3Al_5O_{12}$ nanostructured ceramics (b).

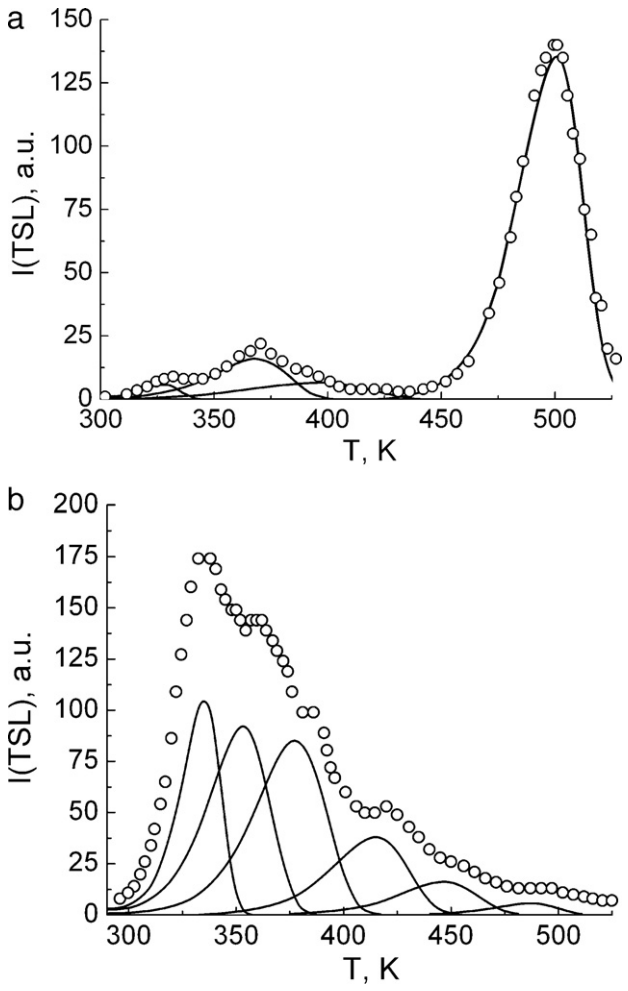

Fig. 6. TSL glow curves of $Y_3Al_5O_{12}$ single crystal (a) and $Y_3Al_5O_{12}$ nanostructured ceramics (b) irradiated with X-ray quanta (9000 R dose). The open circles denote experimental points, the solid lines – fitting by first order kinetics.

irradiation with X-ray quanta (9000 R dose). The deconvolution of experimental plots into elementary peaks was done by GlowFit software assuming first-order kinetics [47]. The TSL curves of $Y_3Al_5O_{12}$ single crystals and nanostructured ceramics are non-elementary and consist of groups of peaks in the 300–525 K temperature range. TSL of single crystal contains several peaks at $T = 330$, 370, 400 and 500 K, idicating the presence of four traps of charge carriers. The activation energy of main TSL peak at $T = 500$ K is 1.55 eV. The glow curve of nanostructured ceramics demonstrates significant distinctions as compared to single crystals and presents superposition of number of peaks quasi-continuously distributed in the $T = 300$–525 K range. Althought at least six peaks can be revealed in the TSL glow-curve, we failed to correctly estimate their energetical parameters because the peaks are strongly overlapped (Fig. 6b). The light sum storaged by nanoceramics is 2.5 times higher than that of single crystals, specifying the higher concentration of point defects trapped the charge carriers.

As known, energy of X-ray quanta ($E = 30$ keV) is insufficient to create stable radiation defect in complex oxides by impact mechanism, because relatively high threshold displacement energy. Formation of displacement defects in $Y_3Al_5O_{12}$ anionic sublattice requires energy of 40 eV [48]. For this reason observed TSL is most likely connected with ''recharging'' of genetic (intrinsic or growth) defects or impurity ions. Strictly speaking, the presence of thermally stimulated luminescence allows only make conclusions about number of defects and their activation energy (location of levels of defects in band gap), not on their nature. Assuming identical radiative recombination mechanisms for both $Y_3Al_5O_{12}$ single crystals and nanostructured ceramics, one can conclude the higher deficiency of nanoceramics. The shape of TSL curve of nanoceramics demonstrates similarity with oxide glasses having quasi-continuous distribution of traps [49]. Numerous grain boundaries, surface states and microstrains presented in nanoceramics leads to redistribution of existing and to creation of new traps not typical for single crystals. After TSL measurements even at relatively low temperatures (constant rate heating up to 525 K) the samples of $Y_3Al_5O_{12}$ nanostructured ceramics become opaque. The loss of transparency can be connected with coagulation of vacancies (presented in relatively high concentration in nanoceramics) with development of large pores or cavities that scatter the light. This mechanism was recently applied to describe degradation of optical properties of YSZ translucent nanoceramics after thermal treatment [13].

4. Conclusions

$Y_3Al_5O_{12}$ nanostructured ceramics having a total transmittance of 63% at $\lambda = 1064$ nm have been produced by low-temperature high-pressure consolidation of co-precipitated nanopowders. The preparation conditions of single-phase translucent ceramics with grain size of 20–40 nm have been determined (a pressure of 7.7 GPa, sintering temperature of 350 °C, sintering time 30–60 s). According to HR TEM, the near pore-free ceramics consists of close-packed crystallites divided by high-angle multifaceted grain boundaries with arbitrary orientated facets. It has been shown that $Y_3Al_5O_{12}$ nanostructured ceramics retain garnet phase and chemical composition and short range ordering of atoms, but has much more defect structure compared to corresponding single crystals. This results in blue shift of transmittance cutoff of nanostructured $Y_3Al_5O_{12}$ in the IR, increase of luminescence intensity of F-like centers and higher intensity of thermally stimulated luminescence. Annealing of $Y_3Al_5O_{12}$ nanoceramics at relatively low temperatures of about 550 K leads to irreversible microstructural changes accompanied by loss of transparency.

Acknowledgments

The work was partially supported by Target Complex Program of Fundamental Research of NAS of Ukraine «Fundamental problems of Nanostructured Systems, Nanomaterials and Nanotechnologies», Project ''Spalakh''. Authors are grateful for Dr. S.N. Nizhankovski, Dr. S.V. Parkhomenko and Dr. D.S. Sofronov for experimental assistance.

References

[1] A. Ikesue, Y.L. Aung, Nat. Photonics 2 (2008) 721–727.
[2] Pat. 3218963 (A) Japan, IC[1-7] C04B35/44, A. Ikesue, Publ. 26.09.91.
[3] Pat. 10101333 (A) Japan, IC[1-7] C04B 35/44; C01F 17/00; H01S 3/16, T. Yanagitani, H. Yagi, M. Ichikawa, Publ. 21.04.98.
[4] Pat. 10101411 (A) Japan, IC[1-7] C04B 35/44; C01F 17/00, T. Yanagitani, H. Yagi, Y. Hiro, Publ. 21.04.98.
[5] Pat. 6825144 B2 USA, IC[7] C04B 35/50, H. Yagi, T. Yanagitani, Publ. 30.11.04.
[6] E. Carnall, D. Pearlman, Mater. Res. Bull. 7 (1972) 647–653.
[7] E. Straßburger, J. Eur. Ceram. Soc. 29 (2009) 267–273.
[8] A. Greskovich, S. Duclos, Annu. Rev. Mater. Sci. 27 (1997) 69–88.
[9] R. Apetz, M.P.B. van Bruggen, J. Am. Ceram. Soc. 86 (2003) 480–486.
[10] A. Krell, T. Hutzler, J. Klimke, J. Eur. Ceram. Soc. 29 (2009) 207–221.
[11] M.A. Meyers, A. Mishra, D.J. Benson, Prog. Mater. Sci. 51 (2006) 427–556.
[12] S.R. Casolco, J. Xu, J.E. Garay, Scripta Mater. 58 (2008) 516–519.
[13] U. Anselmi-Tamburini, J.N. Woolman, Z.A. Munir, Adv. Funct. Mater. 17 (2007) 3267–3273.
[14] B.A. Gizhevskii, Yu.P. Sukhorukov, E.A. Ganshina, N.N. Loshkareva, A.V. Telegin, N.I. Lobachevskaya, V.S. Gaviko, V.P. Pilyugin, Phys. Solid State 51 (2009) 1836–1842.
[15] M.R. Gallas, B. Hockey, A. Pechenik, G.J. Piermarini, J. Am. Ceram. Soc. 77 (1992) 2107–2112.
[16] T.C. Lu, X.H. Chang, J.Q. Qi, X.J. Luo, Q.M. Wei, S. Zhu, K. Sun, J. Lian, L.M. Wang, Appl. Phys. Lett. 88 (2006) 213120 (3 pp.).
[17] J. Zhang, T. Lu, X. Chang, N. Wei, W. Xu, J. Phys. D: Appl. Phys. 42 (2009) 052002 (5 pp.).
[18] J. Zhang, T. Lu, X. Chang, S. Jiang, N. Wei, J. Qi, Nanoscale Res. Lett. 5 (2010) 1329–1332.
[19] R. Fedyk, D. Hreniak, W. Łojkowski, W. Strek, H. Matysiak, E. Grzanka, S. Gierlotka, P. Mazur, Opt. Mater. 29 (2007) 1252–1257.
[20] M. Galceran, M.C. Pujol, P. Gluchowski, W. Strek, J.J. Carvajal, X. Mateos, M. Aguilo, F. Diaz, J. Am. Ceram. Soc. 93 (2010) 3764–3772.
[21] V.S. Kortov, A.E. Ermakov, A.F. Zatsepin, M.A. Uimin, S.V. Nikiforov, A.A. Mysik, V.S. Gaviko, Phys. Solid State 50 (2008) 957–961.
[22] A.A. Makhnev, B.A. Gizhevskii, L.V. Nomerovannaya, J. Exp. Theor. Phys. Lett. 91 (2010) 79–82.
[23] D. Hreniak, W. Strek, P. Głuchowski, R. Fedyk, W. Łojkowski, J. Alloys Compd. 451 (2008) 549–552.

[24] D. Hreniak, M. Bettinelli, A. Speghini, A. Łukowiak, P. Głuchowski, R. Wiglusz, J. Nanosci. Nanotechnol. 9 (2009) 6315–6319.
[25] W. Zhao, D. Hreniak, G. Boulon, W. Strek, A. Brenier, M. Yin, P. Gluchowski, A. Lukowiak, R. Wiglusz, T. Epicier, Radiat. Meas. 45 (2010) 304–306.
[26] V. Pankratov, L. Shirmane, T. Chudoba, P. Gluchowski, D. Hreniak, W. Strek, W. Lojkowski, Radiat. Meas. 45 (2010) 392–394.
[27] T. Yanagida, H. Takahashi, T. Ito, D. Kasama, T. Enoto, M. Sato, S. Hirakuri, M. Kokubun, K. Makishima, T. Yanagitani, H. Yagi, T. Shigeta, T. Ito, IEEE Trans. Nucl. Sci. 52 (2005) 1836–1841.
[28] H. Takahashi, T. Yanagida, D. Kasama, T. Ito, M. Kokubun, K. Makishima, T. Yanagitani, H. Yagi, T. Shigeta, T. Ito, IEEE Trans. Nucl. Sci. 53 (2006) 2404–2408.
[29] I. Kamenskikh, M. Chugunova, S.T. Fredrich-Thornton, C. Pedrini, K. Petermann, A. Vasil'ev, U. Wolters, H. Yagi, IEEE Trans. Nucl. Sci. 57 (2010) 1211–1217.
[30] T.G. Deineka, A.G. Doroshenko, P.V. Mateychenko, A.V. Tolmachev, E.A. Vovk, O.M. Vovk, R.P. Yavetskiy, V.N. Baumer, D.I. Sofronov, J. Alloys Compd. 508 (2010) 200–205.
[31] J.-G. Li, T. Ikegami, J.-H. Lee, T. Mori, J. Am. Ceram. Soc. 83 (2000) 961–963.
[32] D. Hreniak, S. Gierlotka, W. Lojkowski, W. Strek, P. Mazur, R. Fedyk, Solid State Phenom. 106 (2005) 17–22.
[33] M. Akchurin, Sh. Gainutdinov, R.V. Zakalyukin, R.M.A.A. Kaminskii, J. Surf. Invest.: X-ray Synchrotron Neutron Technol. 2 (2008) 716–721.
[34] A. Ikesue, Y.L. Aung, T. Taira, T. Kamimura, K. Yoshida, G.L. Messing, Annu. Rev. Mater. Res. 36 (2006) 397–429.
[35] Sh.M Akchurin, A.A. Kaminskii, Dokl. Phys. 54 (2009) 47–50.
[36] Sh.M. Akchurin, R.M. Zakalyukin, A.A. Kaminskii, I.I. Kupenko, Dokl. Phys. 54 (2009) 367–369.
[37] Yu.N. Barabanenkov, S.N. Ivanov, A.V. Taranov, E.N. Khazanov, H. Yagi, T. Yanagitani, K. Takaichi, J. Lu, J.F. Bisson, A. Shirakawa, K. Ueda, A.A. Kaminskii, J. Exp. Theor. Phys. Lett. 79 (2004) 342–345.
[38] Sh.M. Akchurin, R.V. Gainutdinov, A.A. Kaminskii, A.V. Taranov, E.N. Khazanov, J. Exp. Theor. Phys. 108 (2009) 83–87.
[39] Y. Ishida, H. Ichinose, T. Kizuka, K. Suenaga, Nanostruct. Mater. 6 (1995) 115–124.
[40] H.-E. Schaefer, in: M.A. Nastasi (Ed.), Mechanical Properties and Deformation Behavior of Materials Having Ultrafine Microstructure, Kluwer Academic Press, Dordrecht, 1993, pp. 81–106.
[41] M.M. Braun, L. Pilon, Thin Solid Films 496 (2006) 505–514.
[42] B.A. Gizhevskii, Yu.P. Sukhorukov, A.S. Moskvin, N.N. Loshkareva, E.V. Mostovshchikova, S.V. Naumov, A.M. Balbashov, J. Exp. Theor. Phys. 102 (2006) 297–302.
[43] S.P. Feofilov, Phys. Solid State 44 (2002) 1407–1414.
[44] V. Babin, K. Blazek, A. Krasnikov, K. Nejezchleb, M. Nikl, T. Savikhina, S. Zazubovich, Phys. Status Solidi C 2 (2005) 97–100.
[45] Yu. Zorenko, V. Gorbenko, E. Mihokova, M. Nikl, K. Nejezchleb, A. Vedda, V. Kolobanov, D. Spassky, Radiat. Meas. 42 (2007) 521–527.
[46] Yu. Zorenko, A. Voloshinovskii, V. Savchyn, T. Voznyak, M. Nikl, K. Nejezchleb, V. Mikhailin, V. Kolobanov, D. Spassky, Phys. Status Solidi B 244 (2007) 2180–2189.
[47] M. Puchalska, P. Bilski, Radiat. Meas. 41 (2006) 659–664.
[48] S.B. Ubizskii, A.O. Matkovskii, N. Mironova-Ulmane, V. Skvortsova, A. Suchocki, Y.A. Zhydachevskii, P. Potera, Phys. Status Solidi A 177 (2000) 349–366.
[49] M.F. Dubovik, T.I. Korshikova, Yu.S. Oseledchik, S.V. Parkhomenko, A.L. Prosvirnin, N.V. Svitanko, A.V. Tolmachev, R.P. Yavetskiy, Funct. Mater. 12 (2005) 685–688.